2020

DECOUPLED DIEL SOLUTES: LINKING PRIMARY PRODUCTION AND NITRATE UPTAKE IN A MONTANE STREAM

Kimberly Bray
The University Of Montana

DECOUPLED DIEL SOLUTES: LINKING PRIMARY PRODUCTION AND NITRATE UPTAKE IN A MONTANE STREAM

By

KIMBERLY KAREN BRAY

Bachelor of Science, University of Montana, Missoula, Montana, 2017

Thesis

presented in partial fulfillment of the requirements
for the degree of

Master of Science
in Systems Ecology

The University of Montana
Missoula, MT

December 2020

Approved by:

Scott Whittenburg, Dean of The Graduate School
Graduate School

H. Maurice Valett, Chair
Division of Biological Sciences

Robert O. Hall
Division of Biological Sciences

Payton Gardner
Division of Geosciences

Bray, Kimberly, M.S, Fall 2020 Systems Ecology

Decoupled diel solutes: linking gross primary production and nitrate uptake in a montane stream

Chairperson: H. Maurice Valett

Tight coupling of surface water diel dissolved oxygen (DO) and nitrate-N (NO_3-N) signals reflects stoichiometric demand of carbon and nitrogen in stream ecosystems. However, DO and NO_3-N can become decoupled due to alternative drivers of diel solutes, resulting in conflicting estimates of stoichiometric and modeled NO_3-N uptake. In this study, I measured benthic biomass, hydrology, and dissolved solutes in a montane stream located in western MT over a growing season (June-October 2019). Daily stream metabolism and NO_3-N uptake were modeled using a single-station open-channel approach. Timing and amplitude of key diel signals were characterized quantitatively to assess decoupling of DO and NO_3-N and investigate diel variation in hydrology. I also analyzed the effect of DO and NO_3-N benthic footprint lengths on diel signals. Miller Creek was heterotrophic, with ER ranging from -2.07 ± 0.37 to -5.53 ± 0.11 g O_2 m^{-2} d^{-1} and GPP from 0.03 ± 0.04 to 0.82 ± 0.10 g O_2 m^{-2} d^{-1}. Statistical assessment with generalized additive models (GAMs) tied metabolism to localized channel conditions. Reductions in GPP, water temperature, and hydrology predicted declining ER (R^2_{adj} = 0.72, n = 124, 72.8% deviance explained). ER also decreased with benthic standing stocks, as measured with AFDM (r = -0.74, p = 0.034) and chl *a* (r = -0.92, p = 0.0013), and surface water dissolved organic carbon (DOC) concentration (r = -0.73, p = 0.038). Modeled NO_3-N uptake (3.20 ± 1.50 to 12.14 ± 2.16 mg N m^{-2} d^{-1}) agreed with stoichiometric estimates (0.42 ± 0.05 to 10.10 ± 3.5 mg N m^{-2} d^{-1}) in magnitude, despite clear decoupling of diel DO and NO_3-N signals. GPP, water temperature, surface water flow, and light explained 92.1% of the deviance in modeled NO_3-N uptake (R^2_{adj} = 0.91, n = 110). Daily benthic footprint of NO_3-N ranged from 2.5 to 19.5 km, exceeding that of DO on some sampling days, which varied from 1.2 to 4.1 km. This research provides a model for calculating daily NO_3-N uptake comparable to estimates from stoichiometry using a single-station approach, which can be applied in streams and rivers with diel DO and NO_3-N decoupling.

Introduction

Metabolism in aquatic environments has been the focus of many studies because it links the two major fates of carbon: fixation of carbon dioxide during production and mineralization of organic matter via respiration (Jones and Stanley 2016). Calculating metabolic rates of respiration and production captures heterotrophic and autotrophic energy processing and demand within rivers (Bernhardt et al. 2017). At an ecosystem level, metabolism is measured as gross primary production (GPP), the rate of carbon fixation through chemoautotrophy and photoautotrophy, and ecosystem respiration (ER), the rate of carbon mineralization. Net ecosystem production (NEP) is the difference between GPP and ER. Locally, nitrogen (N) cycling is tightly coupled to carbon processing within streams and rivers due to stoichiometric relationships associated with biotic demand (Redfield 1958, Knops et al. 2002). In most aquatic environments, Nitrate-N (NO_3-N) is the main form of dissolved inorganic N available for biological uptake. As such, exogenous and endogenous factors related to energy flow, including allochthonous resource subsidies and metabolism, influence in-stream NO_3-N retention (Valett et al. 2008). With the advent of autonomous in-situ sensors and sondes, it is now possible to create long-term datasets of daily metabolism (Appling and Heffernan 2014) and nitrate-N (NO_3-N) uptake (Heffernan and Cohen 2010) using fine-scale measurements of diel dissolved oxygen (DO) and NO_3-N signals.

However, modeled estimates of metabolism and uptake may lack anticipated associations due to decoupling of diel NO_3-N and DO signals (Appling and Heffernan 2014, Hensley and Cohen 2016). Here, I define decoupled signals as those that deviate from patterns indicative of autotrophic stoichiometric demand, based on a sinusoidal model. A priori, DO production and NO_3-N depletion over a 24-h period should coincide during peak GPP and autotrophic NO_3-N

uptake, assuming coupled signals represent quotidian processes. As such, diel coupling is characterized by 1) timing of diel NO_3-N minimum and DO maximum (time since midnight at which localized diel minimum/maximum occurred, h) co-occurrence during diurnal hours (Heffernan and Cohen 2010), and 2) increases in diel NO_3-N amplitude (difference between maximum and minimum values within a 24-h period) predicted by increases in DO amplitude (Hensley and Cohen 2016).

Decoupled diel signals may result from in-stream environmental fluctuations, including variable discharge (Brick and Moore 1996, Sullivan et al. 1998) or temperature (Kunz et al. 2017) over 24 h. Alternatively, decoupled DO and NO_3-N can be explained by the respective gaseous and non-gaseous quality of each signal (Hensley and Cohen 2016). Constant re-equilibration of in-stream DO with the atmosphere, and lack thereof for NO_3-N, may very well produce upstream benthic footprints (i.e., spatial extent of stream bottom influencing a given signal) of different lengths and character. As a result, offset, or "smearing", can exist between diel NO_3-N minimum and DO maximum because of varied physical and chemical features reflecting dissimilar reaches of influence.

Previously, Heffernan and Cohen (2010) succcessfully linked GPP and assimilatory autotrophic NO_3-N uptake estimated from diel signals using a single-station open-channel method in a highly productive slow-moving Florida river. However, many of the influences known to decouple solute signals were absent in their study, notably variable benthic footprints of DO and NO_3-N and groundwater-surface water interactions, due to the spring-fed nature of the river. Less is known about using a single-station approach to model assimilatory autotrophic NO_3-N uptake in mid-order creeks that are hydrologically-connected to the aquifer and upstream headwater networks. The main objective of this study was to create a model capable of

accurately estimating daily assimilatory autotrophic NO_3-N uptake from diel signals measured using a single-station approach in a montane creek, as assessed by linkages between modeled NO_3-N uptake and GPP. To do so, I addressed five main goals, including 1) characterizing trends and identifying periods of change in hydrology, metabolism, and NO_3-N uptake, 2) evaluating the relationship between modeled metabolism and assimilatory autotrophic NO_3-N uptake; 3) assessing decoupling of diel NO_3-N and DO signals; 4) analyzing the effect of diel variation in stream flow on solute signals; and 5) evaluate the potential for differences in DO and NO_3-N benthic footprints to explain DO and NO_3-N decoupling.

Materials

Site description

I conducted the study on Miller Creek, a headwater tributary of the Bitterroot River in western Montana, USA. The creek is a snowmelt driven system with spring runoff (1456-2638 L s^{-1}) occurring in April or May, followed by baseflow conditions from August-March (80-200 L s^{-1}). I established an 822-m long study reach approximately 10 km from the creek's headwaters on the MPG Ranch, a 61-km^2 privately-owned property used for a wide range of research purposes, but no active ranching or farming practices. The creek flows through a variety of land-use types, including the Lolo National Forest, and cattle and dry haying operations just upstream of the MPG Ranch. Riparian vegetation along the reach includes grasses and deciduous trees, with a prevalence of dense coniferous cover. Two surface sites (i.e. upstream and downstream) designated reach extent and ten groundwater wells were distributed along its length approximately 1 m from the channel within the riparian zone.

Hydrology & geomorphology

Stream flow in Miller Creek was monitored from June 2017-2019 as part of water quality monitoring program (H.M. Valett, unpublished data) tied to potential restoration actions (Montana DEQ 2018). Discharge was estimated at a single location mid-reach using dilution gauging approaches (Gordon et al. 2004) monthly for the 24-month period.

Beginning in June 2019, surface water discharge (Q, L s^{-1}) and velocity (u, m s^{-1}) were monitored at established upstream and downstream sites using rating curves tied to measurements derived via dilution gauging. At each site, a stilling well equipped with a pressure transducer (kPa; Onset HOBO U20L, Bourne, MA) measured stream stage via water pressure on a five-min interval. Stream stage was corrected for atmospheric pressure measured at each in-stream site (kpa; Solinst Barologger model 3001, Georgetown, ON). Stream discharge was quantified at upstream (n =10) and downstream (n = 6) sites on separate dates from June 13 to October 22 to establish rating curves for each location (r^2 = 0.98-0.99). Herein, channel discharge (Q) is represented by discharge estimated at the downstream site and net groundwater exchange (Q_{gw}, L s^{-1}) calculated as the difference between downstream and upstream flow (L s^{-1}). Wetted width (m) was measured at 25 equally spaced transects within the reach during dilution gauging assessment. Depth (m) was estimated at five-min intervals by dividing Q by the product of width and u.

Modeling ecosystem processes

A Sea-Bird Scientific SUNA V2 sensor (Bellevue, WA) with a detection limit of 4 µg N L^{-1} measured NO_3-N concentration hourly at the downstream surface water site from June 24 to

October 13, 2019. I calculated daily median autotrophic NO_3-N uptake areal flux ($U_{ANO3,}$ mg N m^{-2} d^{-1}) through inverse Bayesian modeling with the *rstan* program in *RStudio 3.6.1*:

$$[N]_i = [N]_{i-1} - \left(\frac{U_{ANO3}}{z_i}\right)\left(\frac{(u_1-u_0)\times PPFD_i}{\sum_{u=1}^{n} PPFD_u}\right) + K_{nit}\,([N]_b - [N]_{i-1})\,(\Delta t) \quad (1)$$

where: [N] is NO_3-N concentration (mg N m^{-3}), i and i-1 are any time step and the preceding timestep, z is stream depth (m), u_0 and u_1 are the beginning and end of any day (h), $PPFD_i$ is photosynthetic photon flux density (PPFD) at each timestep (µmol m^{-2} h^{-1}), $PPFD_u$ is integrated PPFD (µmol m^{-2}) over continuous time u in a day (d), K_{nit} is any daily change in NO_3-N concentration due to loss from autotrophic uptake and denitrification or gains from upstream or groundwater inputs expressed as a rate (d^{-1}), $[N]_b$ is mean daily background concentration (mg N m^{-3}), and Δt is time between i and i-1 (d).

Due to the potential for equifinality, U_{ANO3} was partially pooled with $PPFD_u$ in a linear relationship:

$$U_{ANO3} \sim N\,(\beta_0 + \beta_1 \sum_{u=1}^{n} PPFD_u\ ,\ \sigma_U\ ) \quad (2)$$

Prior of the intercept was $\beta_0 \sim N\,(0, 4.57)$ with prior standard deviation equal to standard deviation of unpooled U_{ANO3} estimates. Prior of the slope of the linear relationship was $\beta_1 \sim TN\,(0, 1 \times 10^{-6})$, based on a half-normal distribution; standard deviation was calculated by dividing the greatest unpooled U_{ANO3} estimate by greatest daily sum of $PPFD_u$. Day-to-day variance in U_{ANO3} from the relationship with light had a prior of $\sigma_U \sim TN\,(0, 4.57)$, with standard deviation also equal to standard deviation of unpooled U_{ANO3}. The model was run with four chains using Hamiltonian Monte Carlo (HMC) methods and 1000 burn-in iterations. Fitted concentration data

from model posterior distribution were qualitatively compared to observed data to assess model fit for each day.

I estimated a prior probability of K~*log N* (2.25, 1.5) from stream NO_3^- uptake and concentration data compiled in Hall et al. (2013) that were collected during more than 30 studies. Using the linear relationship between log-transformed NO_3^- uptake velocities and concentrations, NO_3^- uptake velocity for Miller Creek (m d^{-1}) was estimated from mean concentration measured by the SUNA over the study. Uptake velocity calculated from the linear regression was divided by z to estimate mean K_{nit} prior probability. Standard deviation of K_{nit} prior was equal to the standard deviation of the linear regression model residuals. Background NO_3-N concentration prior probability was $[NO_3\text{-}N]_b$ ~*N* (57.2,12.0), based on average and standard deviation of concentration measured by the SUNA.

Daily metabolism was estimated from June 11 to October 13, 2019 using a single-station open channel method at the downstream site with modeled PPFD (RStudio 3.6.1 *streamMetabolizer* package), z, and DO and water temperature measured on 5-min intervals (Precision Measurement Engineering MiniDOT, Vista, CA). Dissolved oxygen concentration at saturation was calculated from DO and atmospheric pressure to address direction and magnitude of gas exchange. Biological parameters of median daily GPP (g O_2 $m^{-2}d^{-1}$), ER (g O_2 $m^{-2}d^{-1}$), and oxygen gas exchange rate normalized to Schmidt number of 600 (K600, d^{-1}) were estimated with the open source s*treamMetabolizer* package in *RStudio 3.6.1* (Appling et al. 2018). Metabolic prior probabilities were GPP~*N*(3.1, 6) and ER~*N*(-7.1,7.1), based on ranges measured in Hall et al. (2016).

To overcome poor parameter estimation typical of streams with high oxygen reaeration and low metabolism areal fluxes (Appling et al. 2018), K600 variance was partially pooled in a log-

linear relationship with daily Q. Discharge regulates much of the day-to-day variation in K600, with turbulence promoting gas exchange and increased depth reducing it. However, other factors, such as presence of macrophytes, ice, or leaf cover, may also effect K600 (Roberts et al. 2007, Genzoli and Hall 2016). Accordingly, partial pooling of variance reflects the reality that conditions other than Q may change K600 over time. Thus, the prior for K600 was K600~N(*f(discharge)*,0.05), where *f(discharge)* represents a linear relationship between daily K600 and Q. The variance of partial pooling was chosen based on which value produced the least co-linearity between gas exchange and ER. Equifinality was properly addressed, as demonstrated by small covariation between ER and K600 (supporting information Fig. A.1, R^2_{adj} = 0.30, e*df* =3.64, *n* = 125, 32.2% deviance explained).

Gross daily autotrophic uptake ($U_{A;}$ mg N m^{-2} d^{-1}) was estimated from modeled GPP assuming net autotrophic production was equal to 0.5 of GPP (Webster and Meyer 1997) and autotrophic molar C:N was 20 (Hall and Tank 2003). Model-derived daily uptake fluxes (U_{ANO3}, Eq 1) were then compared to those estimated theoretically from GPP (U_A). Following Chapra and Di Toro (1991), the benthic footprints of metabolism and U_{ANO3} were estimated as 3u/K using daily average u and K600 or K_{nit}, respectively.

Light and water chemistry

Water chemistry was measured bi-weekly from June 10 to September 19. Triplicate water samples were collected with HDPE Nalgene containers from the water column at upstream and downstream sites as well as from the ten groundwater wells. Following collection, samples were transported on ice to the laboratory, and filtered (Whatman GF/F, 0.7 µm-pore size) into 15-mL polypropylene tubes for inorganic analytes, or glass containers for dissolved organic carbon (DOC). Samples for inorganic species were frozen (-20˚C) and DOC samples were maintained at 4°C until analysis.

Filtered water samples were analyzed for dissolved NO_3-N (µg L^{-1}), ammonium-N (NH_4-N; µg L^{-1}), and soluble reactive phosphorus (SRP; µg L^{-1}) using an Astoria-Pacific Segmented Flow Analyzer AP2 (Clackamas, OR), and DOC (mg L^{-1}) concentrations via chemical oxidation with a Xylem Aurora 1030W Total Organic C Analyzer (College Station, TX). Nitrate + nitrite was assessed using cadmium-reduction chemistry (U.S. EPA 1993a) with 0.001 N mg L^{-1} detection limit and is reported here as NO_3-N. Soluble reactive phosphorus was assessed following the ascorbic acid colorimetry method with a 0.002 mg P L^{-1} detection limit (U.S. EPA 1993b). Ammonium-N was assessed according to the phenol-hypochlorite colorimetry method (U.S. EPA 1993c) with a 0.005 mg N L^{-1} detection limit. Persulfate oxidation of organic C followed Menzel and Vaccaro (1964) with a detection limit of 0.002 mg C L^{-1}.

Hourly surface incident shortwave radiative flux (W m^{-2}) from the NASA Land Data Assimilation System (NLDAS) data set was converted to PPFD (µmol m^{-2} s^{-1}) using methods described in Yang et al. (2007).

Benthic standing stocks

On a bi-weekly basis concurrent with water sampling, benthic standing stocks were evaluated by randomly collecting three cobbles from the upstream, downstream, and middle of the reach (n = 9/sampling). In the field, epilithic material was removed from the top and sides of each cobble using a wire brush. A homogeneous slurry of individual biomass samples was divided into subsamples, each of which were filtered through a Whatman GF/F glass filter (0.7 µm pore-size). After transport to the lab, filters were frozen (-20˚C) until analysis. Benthic organic matter (BOM) and chlorophyll *a* standing crop (chl *a*, mg m^{-2}) were quantified using filtered material following Steinman et al. (2017). Benthic organic matter was assessed using ash-free dry mass (AFDM, g m^{-2}) while chl *a* was measured spectrophotometrically following acetone extraction and used to represent the abundance of benthic primary producers.

Gas exchange-corrected dissolved oxygen

To explore how much decoupling of DO and NO_3-N signals could be explained by differences in their benthic footprint lengths, I generated a corrected DO signal in which concentration was derived without atmospheric gas exchange. Hourly DO fluxes from the water column associated with gas exchange were calculated and removed from observed DO fluxes leaving only metabolic influences, thereby creating a gas exchange-corrected DO signal (Moore et al. 2011, Hamme et al. 2012). By doing so, I calculated an effectively "nongaseous" DO signal that was produced only from biological consumption or production of DO. Lack of temporal coherence between NO_3-N and gas exchange-corrected DO eliminated difference in NO_3-N and DO benthic footprints as the primary cause of signal decoupling (Hensley and Cohen 2016) .

Statistical analysis

Diel minimum/maximum timing and diel amplitude were quantified for surface water signals each day. I also calculated phase differences between the occurrence of diel DO minimum and NO_3-N maximum (h) to address temporal displacement of signals. Phase differences exceeding 1 h indicated DO and NO_3-N asynchrony (Heffernan and Cohen 2010).

Change over the growing season in and relationships between biweekly variables were analyzed by assessing the fit of linear regression models with Pearson's correlation coefficient (Sokal and Rohlf 1994). Time series of daily observations were modeled using univariate generalized additive models (GAM) with restricted maximum likelihood smoothness selection (REML) and thin plate regression splines via the *mgcv* package in *RStudio 3.6.1* (Simpson 2017). Outliers associated with storm events were removed from Q (n = 1) and Q_{gw} (n = 1) prior to time series analysis. In cases of persistent residual autocorrelation, a continuous-time first- (CAR (1)) or second-order (CAR (2)) autoregressive process was added to the model (Simpson 2018). Best-fit models of time series were chosen based on Akaike information criterion (AIC). Periods of change in modeled time series were identified by points at which the first derivative of the best-fit model with 95% simultaneous confidence interval did not include zero. First derivatives were calculated using the *gratia* package (*RStudio 3.6.1*). Predictors of metabolism and NO_3^- uptake were assessed using uni- and multi-variate GAMs. Since there were fewer observations for daily and diel NO_3-N than other variables, using AIC to assess model fit with predictors was not appropriate; instead, I chose models with greatest deviance explained, adjusted R-squared (R^2_{adj}), and sample size, n (Finlay et al. 2019). In all models, the number of basis functions was selected to promote random distribution of residuals (Simpson 2017).

Results

Daily trends

Daily surface water Q (73.1-365.8 L s^{-1}) rapidly declined from June 10 to July 16 as runoff subsided into baseflow conditions (Fig. 1a, R^2_{adj} = 0.98, e*df* =11.58, *n* = 125). Excluding a late-summer flood event that occurred on September 4 through 7 due to a rainstorm, Q remained stable for the rest of the study (Fig. 1b). During peak runoff, the Miller Creek study reach gained groundwater (supporting information Fig. A.2a, R^2_{adj} = 0.96, e*df* =35.15, *n* = 125), but transitioned to a losing reach on June 20. Daily Q_{gw} peaked at 54.1 ± 2.3 L s^{-1} on June 14, representing a 16.9% increase in flow over the 822 m of stream. According to the best-fit GAM (supporting information Fig. A.2b), Q_{gw} declined from 48.2 ± 1.9 to -8.2 ± 1.5 L s^{-1} from June 15 to June 21 and greatest average daily loss to groundwater (-36.7 ± 1.9 L s^{-1}, 23% of upstream Q) occurred on July 6. Elevated channel Q on September 11 associated with the summer freshet was accompanied by a positive daily Q_{gw} (3.4 ± 1.9 L s^{-1}); excluding this event, Miller Creek remained a losing reach from June 20 to the end of the study (October 13).

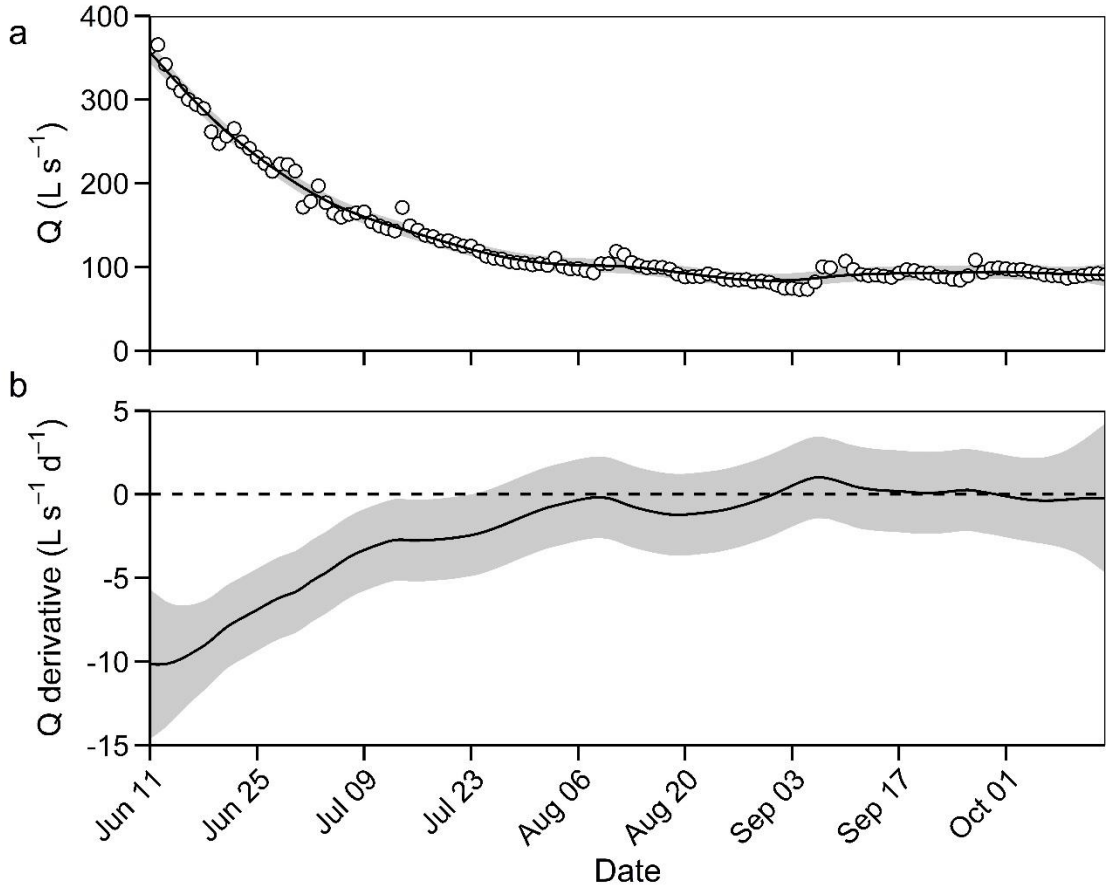

Fig 1. (a) Declining daily surface water discharge (open circles) with best fit GAM (black line) and 95% confidence intervals (gray band) from runoff to baseflow. **(b)** First derivative of GAM (black line) with 95% simultaneous confidence intervals (gray band). Points of change in the modeled time series are indicated by simultaneous confidence intervals that do not include 0.

Average daily DO (supporting information Fig. A.3a) and NO_3-N (supporting information Fig. A.3b) exhibited periods of evident change, but changes did not always align temporally (supporting information Fig. A.4 a-b). Daily DO concentration (8.38-10.4 mg O_2 L^{-1}) remained constant during most of the study, with two periods of increase in late September and early October (R^2_{adj} = 0.93, e*df* =28.91, *n* = 126). In contrast, daily surface water NO_3-N concentration (27.8-102.6 µg NO_3-N L^{-1}) fluctuated more frequently (R^2_{adj} = 0.94, e*df* =29.8, *n* = 112); five periods of increase or decline occurred between August 5 and October 11. Changes in DO and NO_3-N only overlapped on October 10, during which both solutes became more concentrated.

Generally, bi-weekly average concentrations of N, P, and DOC showed no distinct temporal trends over the course of the study (Table 1). Average DOC (0.9-1.8 mg DOC L^{-1}), SRP (3.4 -8.4 µg SRP L^{-1}), and NH_4-N (1.1-19.9 µg N L^{-1}) in surface water did not display temporal trends ($p > 0.05$). Biweekly concentrations estimated from flow injection analysis agreed with SUNA measurements collected within the same hour (±7.6 µg N L^{-1}, ± 8.1 % deviation) indicating high accuracy and precision of SUNA outputs. Additionally, bi-weekly surface water N:P ratios (15.5-51.9) remained above the Redfield ratio of 16. Groundwater N concentrations surpassed those measured in the channel by up to 69.0 µg NO_3-N L^{-1} and 117.6 µg NH_4-N L^{-1}, while SRP and DOC were not as concentrated, with groundwater within 12.3 µg SRP L^{-1} and 6.2 mg DOC L^{-1} of average reach surface water. Groundwater N:P ratios (22.3-197.8) were greater than those for surface water.

Table 1. Bi-weekly reach-scale surface water and groundwater dissolved concentrations and molar N:P ratios. Reach-scale benthic biomass. Data are means ± standard error.

Date	[NO_3-N] (µg N L^{-1})	[NH_4-N] (µg N L^{-1})	[SRP] (µg P L^{-1})	[DOC] (mg L^{-1})	Molar N:P	BOM (g AFDM m^{-2})	Chl *a* (mg m^{-2})
Surface water							
11 June	-	2.2 ± 0.5	5.0 ± 0.9	1.5 ± 0.1	23.0 ± 3.1	16.6 ± 6.9	31.5 ± 12.6
24 June	54.0 ± 0.8	12.0 ± 1.6	5.7 ± 0.6	1.8 ± 0.2	19.4 ± 3.7	13.4 ± 2.2	52.7 ± 17.4
8 July	54.4 ± 1.0	19.9 ± 0.3	5.0 ± 0.4	1.0 ± 0.1	20.9 ± 1.4	9.7 ± 3.4	32.7 ± 14.7
25 July	49.9 ± 1.5	5.3 ± 0.6	5.6 ± 0.8	1.1 ± 0.1	21.7 ± 2.4	12.2 ± 3.9	26.7 ± 12.0
8 August	65.3 ± 1.8	9.5 ± 0.9	8.1 ± 1.2	1.5 ± 0.1	15.5 ± 2.1	7.1 ± 2.3	17.6 ± 4.8
19 August	63.1 ± 1.8	9.5 ± 1.0	8.4 ± 0.4	0.9 ± 0.1	18.0 ± 1.3	5.1 ± 1.5	20.3 ± 9.0
3 September	77.0 ± 1.6	12.5 ± 1.0	3.4 ± 0.5	1.3 ± 0.1	51.9 ± 3.0	3.1 ± 0.5	7.9 ± 3.9
17 September	63.4 ± 1.2	1.1 ± 0.7	3.5 ± 0.5	1.5 ± 0.1	40.8 ± 4.0	5.9 ± 0.9	22.0 ± 9.1
Groundwater							
11 June	83.6 ± 23.9	34.9 ± 13.6	17.2 ± 6.4	7.1 ± 2.8	32.0 ± 16.8	-	-
24 June	96.0 ± 24.3	101.2 ± 32.1	10.0 ± 1.4	3.4 ± 0.5	22.3 ± 3.3	-	-
8 July	106.3 ± 28.6	137.5 ± 37.5	5.8 ± 0.5	7.2 ± 3.8	186.9 ± 41.5	-	-
-25 July	119.5 ± 25.7	68.7 ± 14.2	5.4 ± 0.6	2.0 ± 0.2	197.8 ± 49.0	-	-
8 August	101.8 ± 18.5	80.9 ± 17.8	10.1 ± 1.3	1.7 ± 0.2	43.6 ± 5.0	-	-
19 August	122.9 ± 19.7	65.8 ± 11.1	10.2 ± 1.4	1.2 ± 0.1	48.2 ± 6.7	-	-
3 September	116.2 ± 17.2	48.5 ± 10.3	6.0 ± 1.2	1.6 ± 0.1	101.8 ± 34.4	-	-
17 September	106.0 ± 16.4	63.6 ± 20.4	6.7 ± 1.5	1.7 ± 0.1	98.9 ± 24.4	-	-

Benthic standing stocks and stream metabolic behavior

Miller Creek was strongly heterotrophic, with median daily GPP (Fig. 2a) ranging from 0.03 ± 0.04 to 0.82 ± 0.102 g O_2 m^{-2} d^{-1} and ER (Fig. 2a) from -2.07 ± 0.37 to -5.53 ± 0.11 g O_2 m^{-2} d^{-1}. On any given day during the study, ER was at least six times greater than GPP, resulting in negative daily NEP (-1.87 ± 0.01 g O_2 m^{-2} d^{-1}) and P:R ratios far less than 1 (0.01-0.16). GPP did not change from June through October (Fig. 2b, R^2_{adj} = 0.55, e*df* =5.11, *n* = 125). ER decreased from June 19 to July 26 (Fig. 2c, R^2_{adj} = 0.57, e*df* =3.06, *n* = 125) beginning during the noted period of reduction in surface water flow. Average BOM ranged from 3.1-16.6 g AFDM m^{-2} and chl *a* standing crop was 7.9-52.7 mg m^{-2} (Table 1). Both BOM (*r* = -0.91, *p* = 0.0019) and chl *a* (*r* = -0.75, *p* = 0.032) declined from June to October and metrics of standing stocks were positively related (*r* = 0.75, *p* = 0.032).

Despite lacking coinciding points of change in metabolic time series, ER and was tied to standing stocks and local conditions in the channel, indicating modeled metabolism reflected endogenous controls. ER magnitude increased with chl *a* (supporting information Fig. A.5a, *r* = -0.92, *p* = 0.0013), AFDM (supporting information Fig. A.5b, *r* = -0.74, *p* = 0.034), and downstream DOC concentration (supporting information Fig. A.5c, *r* = -0.73, *p* = 0.038). In contrast, GPP was not related to the abundance of epilithic autotrophs (*p* = 0.084) or BOM standing stocks (*p* = 0.19). Additionally, GPP could not be tied to biweekly measurements of SRP (*p* = 0.64), NH_4-N (*p* = 0.67), or DOC (*p* = 0.26). In the best-fit multi-variate GAM, decreases in GPP, water temperature, and Q predicted reduced ER (R^2_{adj} = 0.72, *n* = 124, 72.8% deviance explained).

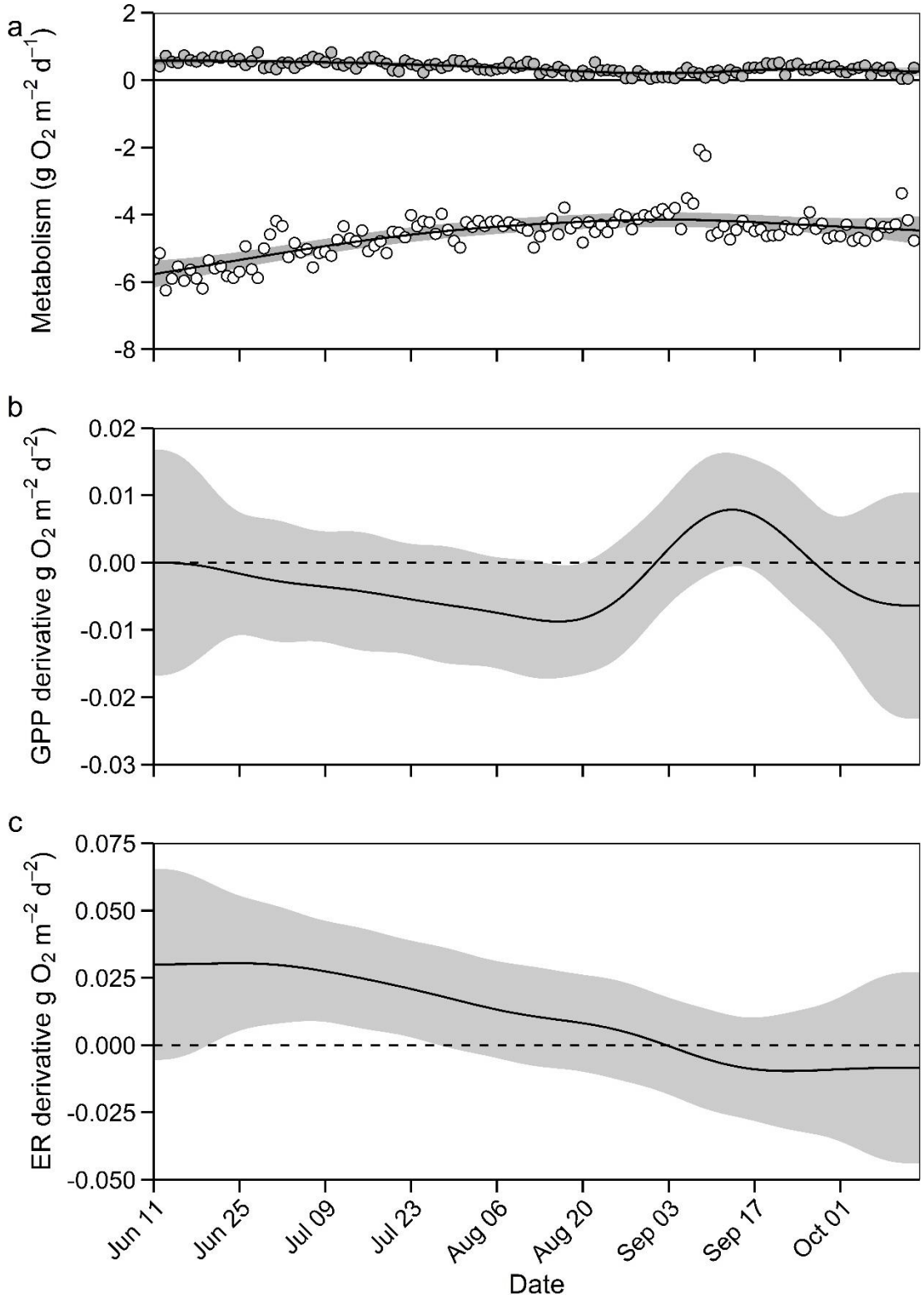

Fig 2. (a) Daily GPP (gray circles) and ER (open circles) with best fit models (black line) and 95% confidence interval (gray band) over the study. First derivatives (black line) with 95% simultaneous confidence intervals (gray band) show **(b)** no periods of change in GAM of GPP and **(c)** early summer decreases in negative ER.

Nitrate uptake

Pooling U_{ANO3} with daily light (Fig. 3a) reduced day-to-day variation in U_{ANO3} compared to the unpooled model (Fig. 3b) and resulted in negligible covariance between U_{ANO3} and K_{nit} (Fig. 3c), a key requirement for parameter estimation. Daily median pooled uptake (U_{ANO3}) ranged from 3.20 ± 1.50 to 12.14 ± 2.16 mg N m^{-2} d^{-1}. Mean daily K_{nit} ranged from 2.73 to 18.98 d^{-1}, exceeding the prior on 30 of 111 days indicating parameter estimates of K_{nit} were not solely dependent on prior probability (Fig. 3d). Pooled U_{ANO3} agreed with those estimated from GPP (U_A). Stoichiometric uptake ranged from 0.42 ± 0.05 to 10.10 ± 3.5 mg N m^{-2} d^{-1} (Fig. 4a), comparable in magnitude to U_{ANO3}. Furthermore, the best-fit multi-variate GAM indicated that GPP, water temperature, surface water Q, and light explained 92.1% of the deviance in U_{ANO3} (R^2_{adj} = 0.91, n = 110), with decreases in the magnitude of all predictors resulting in declines in U_{ANO3}. GPP alone explained 21.0% of the deviance in U_{ANO3} (Fig. 4b, univariate model, R^2_{adj} = 0.20, n = 111).

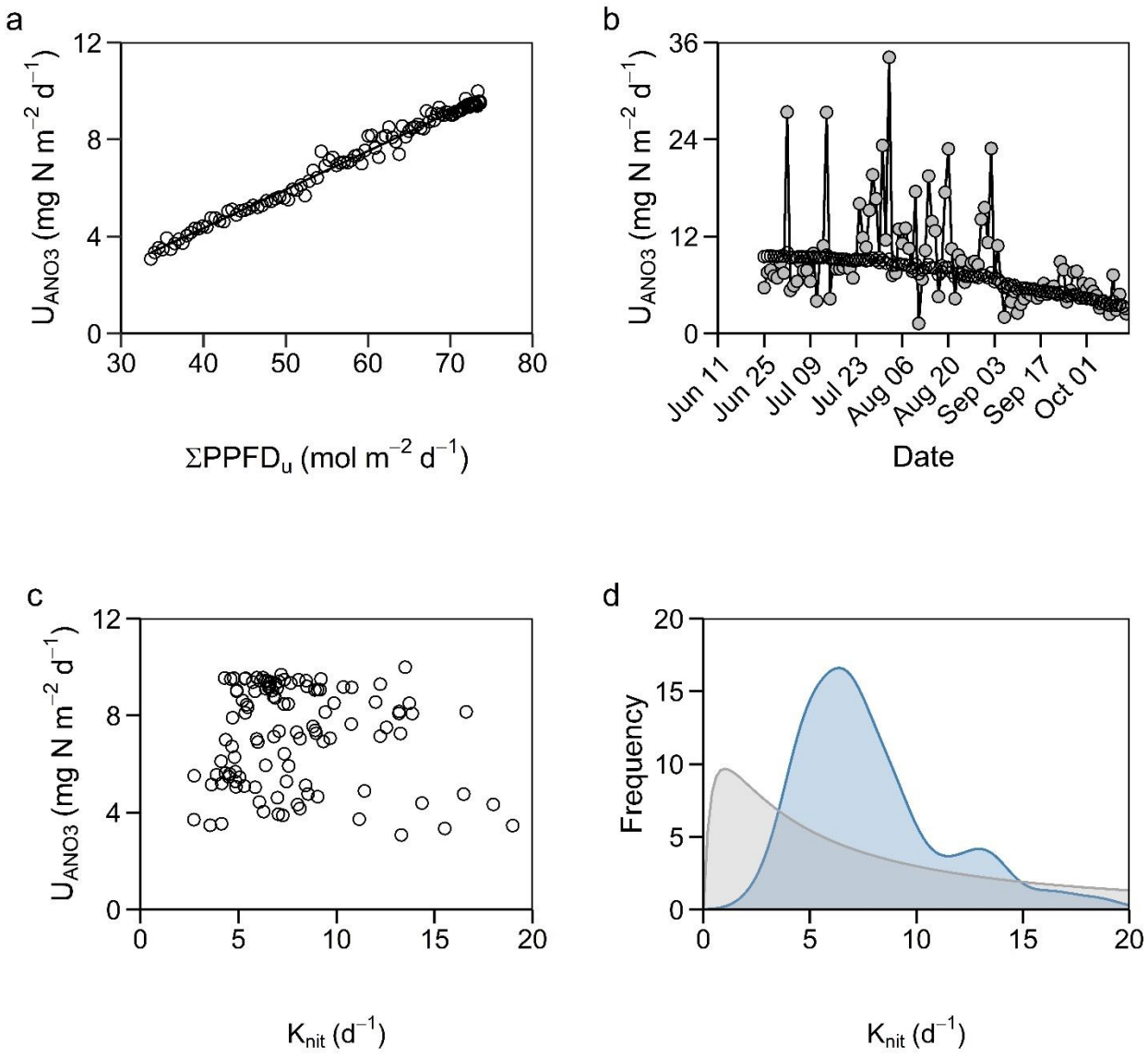

Fig 3. (a) Pooled U_{ANO3} and total daily light over the study. Line indicates linear relationship used to model U_{ANO3} from light. **(b)** Pooled U_{ANO3} with light (open circles) reduced day-to-day variability compared to unpooled (gray circles) estimates. **(c)** Lack of covariance between pooled U_{ANO3} and K_{nit} over the study period. **(d)** Distribution of estimated K_{nit} parameters (blue) varied from log-linear prior probability distribution (gray).

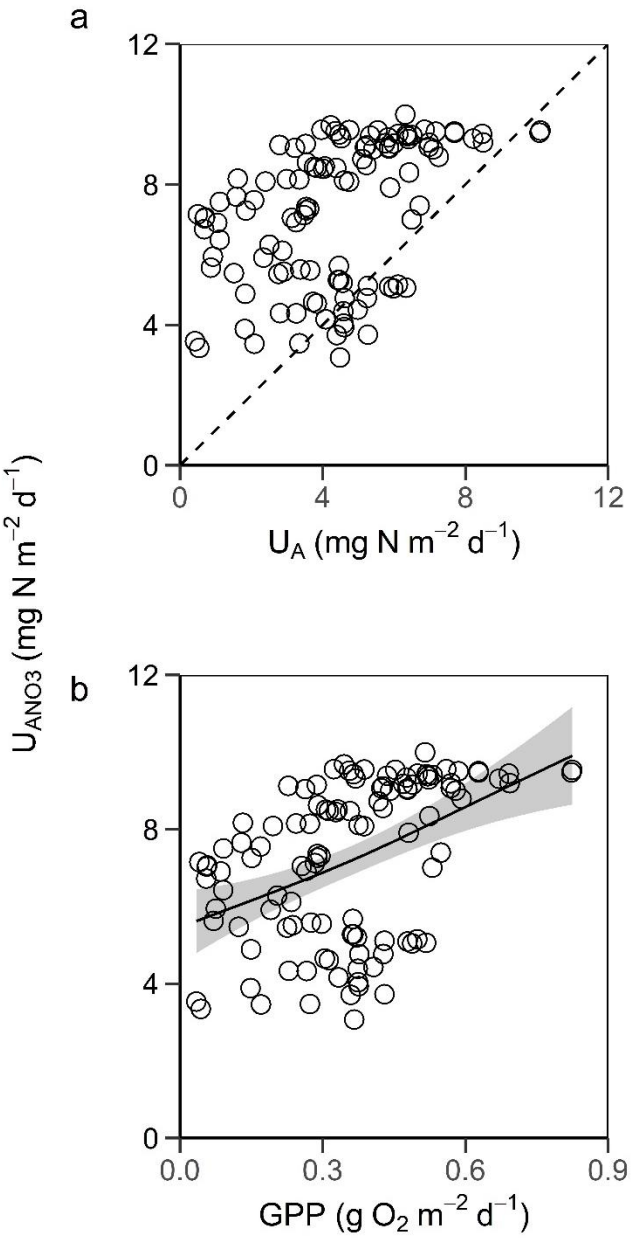

Fig 4. (a) Modeled (U_{ANO3}) and stoichiometric (U_A) estimates of NO_3-N uptake were similar in magnitude, as compared with a 1:1 line (dashed line). **(b)** Best-fit GAM (black line) with 95% confidence intervals (gray bands) describing relationship between U_{ANO3} and GPP (open circles).

Diel signals

As stream flow declined from runoff to baseflow, 24-h change in Q followed suit. Diel amplitude of Q decreased from 240 L s^{-1} on June 11 to 13.3 L s^{-1} on October 13 (R^2_{adj} = 0.52, e*df* =1.16, *n* = 123). Timing of Q diel minimum and maximum lacked coherent patterns over the entire study. Diel Q maxima were typically noted during daylit hours in the morning or early afternoon (7:09-17:54, n = 101) and minima during late afternoon or night (16:44-23:54, *n* = 89). However, there were also days during which maxima occurred in the early morning or night (*n* = 24) and minima in the early morning (0:05-8:55, *n* = 38). Although diel Q_{gw} amplitude declined slightly from June to October (R^2_{adj} = 0.59, e*df* =6.14, *n* = 121), there were no notable periods of change in the modeled time series. Timing of diel Q_{gw} minimum (0:00-23:41) and maximum (0:01-23:59) did not follow distinct diel patterns.

Like trends noted in daily averages, growing season patterns in the amplitude and timing of diel DO and NO_3-N concentrations did not align as anticipated. According to the best-fit GAM, diel DO amplitude ranged from 0.32-1.59 mg L^{-1} (supporting information Fig. A.6a-b, R^2_{adj} = 0.22, e*df* =5.91, *n* = 125) but did not vary from June to October. Amplitude of diel change in NO_3-N concentrations ranged from 8.5-36.8 µg NO_3-N L^{-1}, increasing from 20.8 to 25.9 µg NO_3-N L^{-1} over 12 days from July 13 to 24 (supporting information Fig. A.7a-b, R^2_{adj} = 0.33, e*df* = 4.113, *n* = 111). DO concentration was lowest in the late-afternoon or evening (14:21-23:17), not during pre-dawn hours as expected from metabolic patterns alone. Maximum DO concentration was recorded in the morning or mid-afternoon (8:11-14:17) and occurred later in the day as summer advanced (supporting information Fig. A.8a-b, R^2_{adj} = 0.40, e*df* = 1.14, *n* = 125). NO_3-N minima were far more broadly distributed, ranging from predawn hours to evening (1:00-21:00), and did not shift directionally with time (supporting information Fig. A.9a-b, R^2_{adj} = 0.12, e*df* =

4.13, n = 111). In contrast to the timing of DO and NO_3-N minima, maximal diel NO_3-N was more tightly constrained, measured between 23:00-0:00.

Decoupled nitrate and dissolved oxygen

Diel patterns expected for NO_3-N and DO due to mechanistic coupling of in-stream biological processing were not observed (Fig. 5a-b). Diel DO amplitude did not predict diel NO_3-N amplitude (R^2_{adj} = 0.016, deviance explained =3.55 %, n = 111) nor did the diel timing of maximum DO relate to minimum NO_3-N (R^2_{adj} = -0.0015, deviance explained =1.22 %, n = 111). Phase differences reflecting discordance between diel DO maxima and NO_3-N minima ranged from 1 min to as much as 11 h 3 min, with an average of 2 h 53 min.

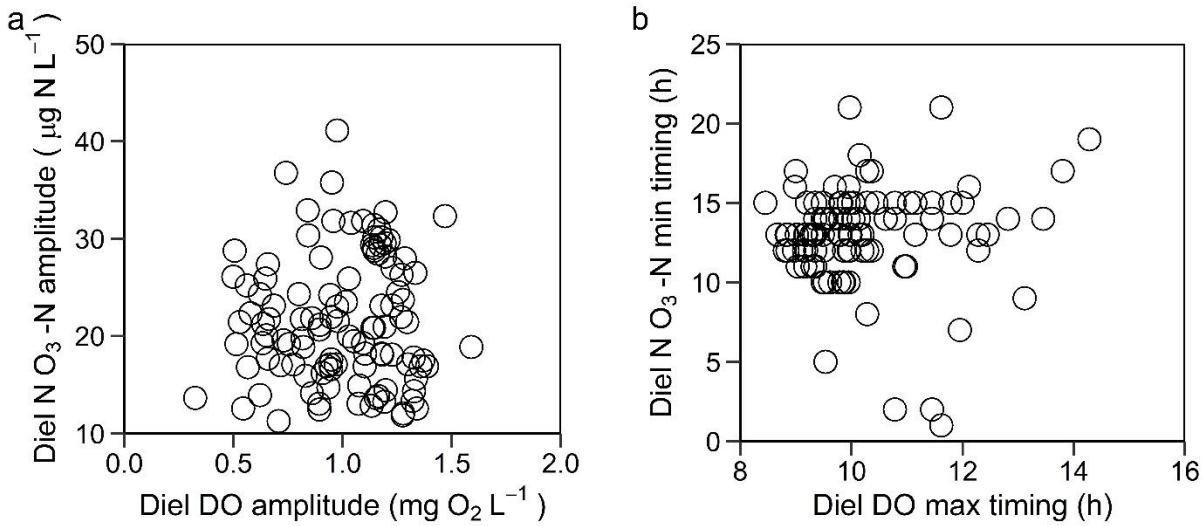

Fig 5. Lack of predictability between **(a)** Diel DO and NO_3-N amplitudes and **(b)** diel DO maximum and NO_3-N minimum timing indicated decoupling between the solute signals.

Variation in flow over 24-h could not account for the diel character of solute signals nor the asynchrony between those for NO_3-N and DO. Diel Q amplitude did not predict diel NO_3-N amplitude (R^2_{adj} = -0.0083, deviance explained =0.12 %, n = 109). If diel variation in Q_{gw} were assumed to drive 24-h changes in NO_3-N, then inflow of water void of N would need to have ranged from 19.9 to 115.8 L s^{-1}, which occurred on only 15 of 113 d during SUNA deployment. At the same time, local hydrometrics indicated that over most of the study the designated reach lost water to the alluvial aquifer, making dilution or enrichment due to groundwater discharge locally inapplicable. Additionally, timing of diel NO_3-N minima was not tied to the occurrence of Q maxima (R^2_{adj} = -0.0078, deviance explained =0.15 %, n = 110), further pointing towards an absence of connection between diel hydrology and NO_3-N concentration.

Overall, removing the effects of gas exchange decreased daily DO concentration as expected given the consistently undersaturated (88.7-92.2% saturation) status of surface water. The magnitude of decline in daily average, however, was relatively small (0.06-1.14 mg O_2 L^{-1}), and average diel amplitude decreased by only 0.03 mg L^{-1}. Correcting DO for gas exchange did not remove phase difference between diel NO_3-N minima and DO maxima (Fig. 6a-c). Reductions in lag times of up to 5 h 10 min were noted as a result of correcting for gas exchange, but this adjustment also amplified the phase difference on some days by as much as 10 min. Average phase difference post correction was 2 h 35 min, only 18 min shorter than the average phase difference prior to gas exchange removal, and still in exceedance of differences indicative of coupled signals. Furthermore, gas exchange-corrected DO diel maxima did not predict NO_3-N minima (R^2_{adj} = 0.014, deviance explained = 2.91 %, n = 111), nor did diel amplitude of DO post-correction predict NO_3-N diel amplitude (R^2_{adj} = -0.00543, deviance explained = 0.36 %, n = 111).

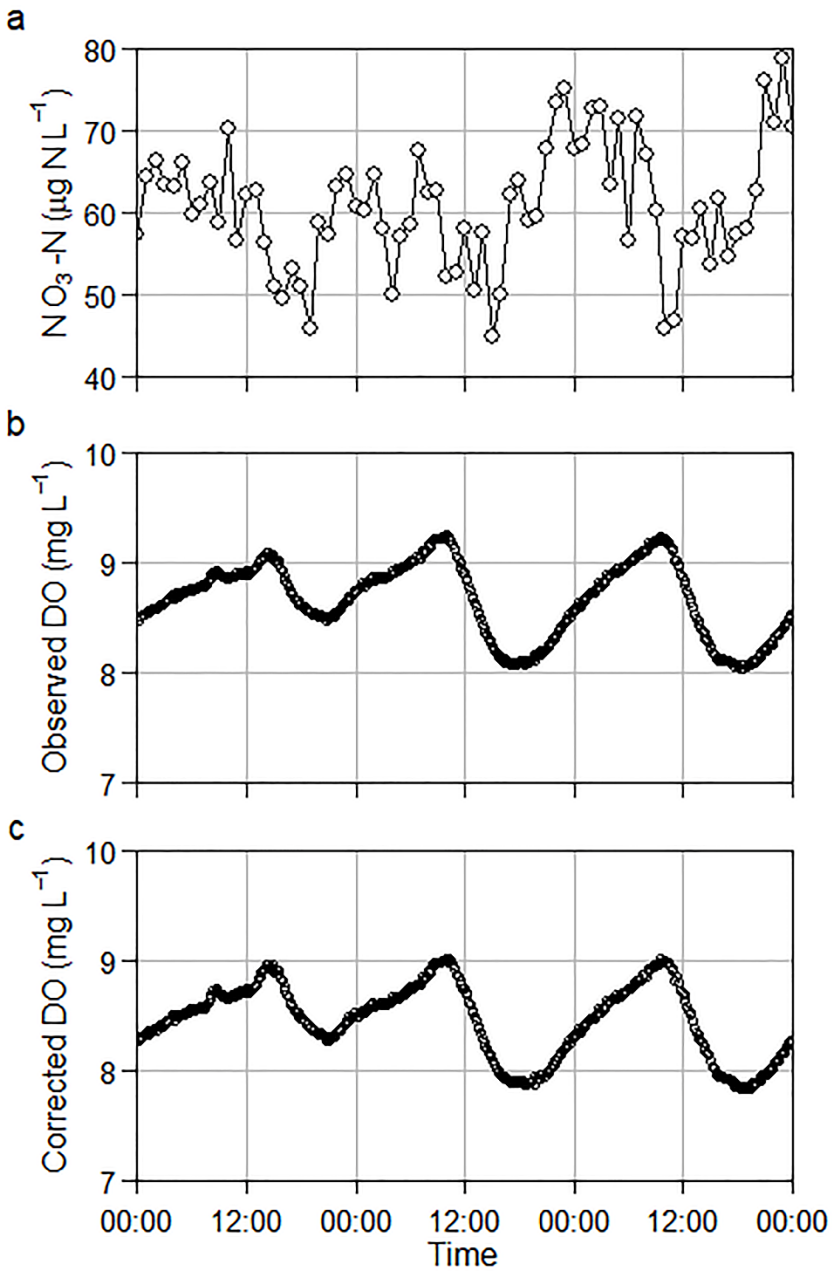

Fig 6. Concentrations over three days of sampling (August 17 00:00 to August 20 00:00) illustrating diel patterns of **(a)** NO_3-N, (**b**) observed DO, and **(c)** gas-exchange-corrected DO concentrations.

Benthic footprints

According to estimates of benthic footprint lengths, the potential integration distance of diel NO_3-N signal was slightly longer than that of DO on all sampling days. Benthic footprint of NO_3-N ranged from 2.5 to 19.5 km, in some cases exceeding the distance to Miller Creek's headwaters from the MPG study reach. Benthic footprint of DO varied less than that of NO_3-N, ranging from 1.2 to 4.1 km. Difference in length between benthic footprints of solutes explain only 1.89 % of deviance in differences between modeled and stoichiometric daily uptake (R^2_{adj} = 0.01, n = 111) and 22.2 % of deviance in the phase difference between timing of NO_3-N minimum and DO maximum (R^2_{adj} = 0.19, n = 111).

Discussion

By using diel signals measured with a single-station open-channel method, I successfully modeled U_{ANO3} estimates that agreed with U_A in magnitude despite the apparent presence of decoupled DO and NO_3-N signals. Pooling diel changes in NO_3-N due to assimilatory autotrophic uptake with light reduced variation in U_{ANO3} and produced estimates closer to those calculated stoichiometrically from GPP. There was no evidence that variation in flow, nor differences in benthic footprints, caused solute decoupling. This work supports findings showing links between in-stream primary production and N uptake (Hall and Tank 2003, Heffernan and Cohen 2010), while providing methodology for assessing biological N use in streams with Bayesian modeling techniques.

Linking modeled and stoichiometric nitrate uptake

The assumption that amplitude of diel signals in channel water reflects in-stream processing allows for the calculation of endogenous benthic uptake (Mulholland et al. 2006, Heffernan and

Cohen 2010). Fluxes of GPP in Miller Creek are in the range of those expected for forested streams (Webster and Meyer 1997) and those seen in natural reference streams studied in the LINX II project (Bernot et al. 2010). U_A derived from these fluxes are comparable to modeled N uptake measures from other systems (Bernhardt et al. 2002). Absolute magnitudes for N uptake derived from metabolic measures are notoriously sensitive to efficiency factors employed to couple C and N dynamics (Hall and Tank 2003, Valett et al. 2008). Despite the propensity for large margins of error to be associated with stoichiometric estimates of N uptake due to gross approximation of efficiency errors, assimilatory autotrophic NO_3-N uptake fluxes calculated stoichiometrically from GPP (U_A) and modeled using the Bayesian approach (U_{ANO3}) differed only by 0.08 to 6.65 mg N m^{-2} d^{-1} (a factor of 0.68 to 14.3) in Miller Creek. Furthermore, despite no variation in GPP over the study, GPP still partially explained U_{ANO3}. Based on these findings, I conclude that I devised a model capable of estimating N uptake than can be linked to GPP in Miller Creek and similar streams. However, application of the model may be limited to a specific range of NO_3-N concentration. Issues may arise if the model is applied in streams with high NO_3-N concentrations, as diel signal smearing is likely to occur (Hensley and Cohen 2020). In addition, if NO_3-N concentrations are limiting, the diel signal may fail to reflect declines in concentration during the day due to U_{ANO3} (Chamberlin et al. 2019).

Hydrology and diel variation in NO_3-N

While diel patterns in solutes often results from variation in flow over 24-h (Brick and Moore 1996, Sullivan et al. 1998), this does not appear to be the case for diel amplitudes in NO3-N concentrations in Miller Creek. Diurnal NO_3-N reductions could hypothetically result from dilution via surface water mixing with N-poor sources during the day. However, it is unlikely that diel reductions in NO_3-N were the result of daytime groundwater inflow. Calculated Q_{gw}

indicated that water was leaving the channel within the reach during most of SUNA deployment; additionally, groundwater was N-rich compared to surface water. While it is possible that the upstream benthic footprint of in-stream processes influencing diel amplitude (i.e., U_{ANO3}) encompassed gaining reaches above the study reach, diel increases in surface water Q necessary to dilute NO_3-N by the measured diel concentration were rarely achieved. Alternatively, variable exogenous N sources could drive changes in channel N concentrations. For instance, upstream inputs fluctuations associated with irrigation altering NO_3-N concentration over 24 h as has been suggested for other systems (Harrison et al. 2005) . However, as argued by Parker et al. (2010), consistent diel changes are unlikely to be linked to irrigation practices that are typically far less temporally coherent and timing of diel Q minima and maxima would likely not be as uniform as observed for Miller Creek. Therefore, I conclude that diel NO_3-N patterns were largely independent from changes in groundwater or surface water hydrology over 24-h.

Alternatively, NO_3-N removal from the channel via hyporheic exchange with the stream could feasibly produce slight differences in U_A and U_{ANO3} measures. Recent publications have suggested that physical retention may play a greater role in reach N retention than previously thought (Emanuel et al. 2014, Woelber et al. 2018). If sufficient surface water-hyporheic exchange with spatially appropriate scales integrates water with distinctly different N concentrations, then surface water could change in concentration upon reentering the channel due to mixing with alternative flow paths. Although this may explain why U_{ANO3} was typically slightly greater than U_A, it is difficult to see how this manner of retention would produce phase differences between NO_3-N and DO signals such as those seen in Miller Creek.

Are diel NO_3-N signals reflective of localized instream processes?

Continuing to operate under the assumption of in-stream control, three mechanisms may explain decoupling between DO and NO_3-N signals from patterns expected due to biological demand of solutes. First, GPP and assimilatory autotrophic N uptake may not cooccur. This is highly unlikely, however, given the well documented temporal association between assimilatory autotrophic N uptake and GPP in streams (Roberts and Mulholland 2007, Valett et al. 2008), lakes (Murphy 1980, Dodds et al. 1989) and oceanic environments (Smith and Hollibaugh 1993, Falkowski et al. 1998) due to stoichiometric demand. Alternatively, differences in upstream integration distances (i.e., footprints) between solutes can cause mismatch between DO and NO_3-N signals (Hensley and Cohen 2016). Assuming that changing NO_3-N concentrations reflected quotidian shifts occurring further upstream than those for DO, diel signal propagation downstream (Wondzell et al. 2007) could explain the lag time between diel minimum NO_3-N and maximum DO concentration in Miller Creek. However, the benthic footprint for NO_3-N was longer than DO by an average factor 4.6, a relatively small difference in length. Moreover, differences in benthic footprints of U_A and U_{ANO3} did not explain variation between empirical and stoichiometric uptake estimates. Removing the influence of gas exchange on DO signals did not eliminate lag between diel DO maxima and NO_3-N minima. Signal mismatch after isolating metabolic DO production and consumption from gas exchange further suggests that signal divergence was not caused by the molecular properties of DO and NO_3-N. These results agree with findings from Greiwe et al. (2020), who concluded that diel NO_3-N signals are reflective of localized instream processes despite the potential for large streambed integration distances due to the nongaseous nature of NO_3-N.

Finally, diel variation in biological NO_3-N consumption via alternative pathways to assimilatory autotrophic uptake could decouple NO_3-N and DO diel signals. A key assumption made in modeling U_{ANO3} stipulated that changes in the diel NO_3-N signal during daylit hours resulted from assimilatory biological use by autotrophs. However, previous publications have shown that denitrification can vary drastically over 24-h (Harrison et al. 2005, Hensley and Cohen 2020). Furthermore, increased nitrification during the day in stream sediments due to warm temperatures may promote denitrification (Lorenzen et al. 1998), resulting in the co-occurrence of diurnal assimilatory autotrophic uptake and denitrification amplification. If denitrification was strongly dependent on nitrification in Miller Creek, diurnal changes in NO_3-N would reflect not only assimilatory autotrophic uptake, but a convolution of signals from 24-h variation in autotrophic and heterotrophic processes that influence NO_3-N abundance. However, timing of diel NO_3-N maximum was not characteristic of signals resulting from high assimilatory autotrophic uptake and denitrification during the day, in which maxima occur midday or evening (Greiwe et al. 2020).

Implications for modeling NO_3^- uptake from diel signals

This study provides methodology that allows for estimation of N uptake and metabolism at similar spatial scales using a single-station approach. The application of a Bayesian modeling method produced estimates of NO_3^- uptake that agreed in magnitude to those calculated from GPP despite the presence of decoupled NO_3-N and DO solutes. Consequently, these results provide insights into modeling techniques for N uptake in creeks that are highly interconnected with their watershed through hydrologic linkages for much of the year.

References

Appling, A. P., R. O. Hall, C. B. Yackulic, and M. Arroita. 2018. Overcoming Equifinality: Leveraging Long Time Series for Stream Metabolism Estimation. Journal of Geophysical Research: Biogeosciences 123:624–645.

Appling, A. P., and J. B. Heffernan. 2014. Nutrient limitation and physiology mediate the fine-scale (DE)coupling of biogeochemical cycles. American Naturalist 184:384–406.

Bernhardt, E. S., R. O. Hall, and G. E. Likens. 2002. Whole-system estimates of nitrification and nitrate uptake in streams of the Hubbard Brook Experimental Forest. Ecosystems 5:419–430.

Bernhardt, E. S., J. B. Heffernan, N. B. Grimm, E. H. Stanley, J. W. Harvey, M. Arroita, A. P. Appling, M. J. Cohen, W. H. McDowell, R. O. Hall, J. S. Read, B. J. Roberts, E. G. Stets, and C. B. Yackulic. 2017. The metabolic regimes of flowing waters. Limnology and Oceanography 63:S99–S118.

Bernot, M. J., D. J. Sobota, R. O. Hall, P. J. Mulholland, W. K. Dodds, J. R. Webster, J. L. Tank, L. R. Ashkenas, L. W. Cooper, C. N. Dahm, S. V. Gregory, N. B. Grimm, S. K. Hamilton, S. L. Johnson, W. H. McDowell, J. L. Meyer, B. Peterson, G. C. Poole, H. M. Maurice Valett, C. Arango, J. J. Beaulieu, A. J. Burgin, C. Crenshaw, A. M. Helton, L. Johnson, J. Merriam, B. R. Niederlehner, J. M. O'Brien, J. D. Potter, R. W. Sheibley, S. M. Thomas, and K. Wilson. 2010. Inter-regional comparison of land-use effects on stream metabolism. Freshwater Biology 55:1874–1890.

Brick, C. M., and J. N. Moore. 1996. Diel variation of trace metals in the upper Clark Fork River, Montana. Environmental Science and Technology 30:1953–1960.

Chamberlin, C. A., E. S. Bernhardt, E. J. Rosi, and J. B. Heffernan. 2019. Stoichiometry and daily rhythms: experimental evidence shows nutrient limitation decouples N uptake from photosynthesis. Ecology 100:1–7.

Chapra, S. C., and D. M. Di Toro. 1991. Delta Method For Estimating Primary Production, Respiration, And Reaeration In Streams. Journal of Environmental Engineering 117:640–655.

Dodds, W. K., K. R. Johnson, and J. C. Priscu. 1989. Simultaneous Nitrogen and Phosphorus Deficiency in Natural Phytoplankton Assemblages: Theory, Empirical Evidence, and Implications for Lake Management. Lake and Reservoir Management 5:21–26.

Emanuel, R. E., A. G. Hazen, B. L. Mcglynn, and K. G. Jencso. 2014. Vegetation and topographic influences on the connectivity of shallow groundwater between hillslopes and streams. Ecohydrology 7:887–895.

Falkowski, P. G., R. T. Barber, and V. Smetacek. 1998. Biogeochemical controls and feedbacks on ocean primary production. Science 281:200–206.

Finlay, K., R. J. Vogt, G. L. Simpson, and P. R. Leavitt. 2019. Seasonality of pCO 2 in a hard-water lake of the northern Great Plains: The legacy effects of climate and limnological conditions over 36 years. Limnology and Oceanography 64:S118–S129.

Genzoli, L., and R. O. Hall. 2016. Shifts in Klamath River metabolism following a reservoir cyanobacterial bloom. Freshwater Science 35:795–809.

Gordon, N. D., T. A. McMahon, B. L. Finlayson, C. J. Gippel, and R. J. Nathan. 2004. Stream hydrology: an introduction for ecologists. West Sussex, UK.

Greiwe, J., M. Weiler, and J. Lange. 2020. Diel patterns in nitrate concentration suggest importance of microbial pathways for in-stream processing:1–20.

Hall, R. O., M. A. Baker, E. J. Rosi-Marshall, J. L. Tank, and J. D. Newbold. 2013. Solute-specific scaling of inorganic nitrogen and phosphorus uptake in streams. Biogeosciences 10:7323–7331.

Hall, R. O., and J. L. Tank. 2003. Ecosystem Metabolism Controls Nitrogen Uptake in Streams in Grand Teton National Park, Wyoming. Limnology and Oceanography Limnol. Oceanogr 48:1120–1128.

Hall, R. O., J. L. Tank, M. A. Baker, E. J. Rosi-Marshall, and E. R. Hotchkiss. 2016. Metabolism, Gas Exchange, and Carbon Spiraling in Rivers. Ecosystems 19:73–86.

Hamme, R. C., N. Cassar, V. P. Lance, R. D. Vaillancourt, M. L. Bender, P. G. Strutton, T. S. Moore, M. D. DeGrandpre, C. L. Sabine, D. T. Ho, and B. R. Hargreaves. 2012. Dissolved O2/Ar and other methods reveal rapid changes in productivity during a Lagrangian experiment in the Southern Ocean. Journal of Geophysical Research: Oceans 117:1–19.

Harrison, J. A., P. A. Matson, and S. E. Fendorf. 2005. Effects of a diel oxygen cycle on nitrogen transformations and greenhouse gas emissions in a eutrophied subtropical stream. Aquatic Sciences 67:308–315.

Heffernan, J. B., and M. J. Cohen. 2010. Direct and indirect coupling of primary production and diel nitrate dynamics in a subtropical spring-fed river. Limnology and Oceanography 55:677–688.

Hensley, R. T., and M. J. Cohen. 2016. On the emergence of diel solute signals in flowing waters. Water Resources Research 52:759–772.

Hensley, R. T., and M. J. Cohen. 2020. Nitrate depletion dynamics and primary production in riverine benthic chambers. Freshwater Science 39:169–182.

Jones, J. B., and E. H. Stanley, editors. 2016. Stream Ecosystems in a Changing Environment. Academic Press, London.

Knops, J. M. H., K. L. Bradley, and D. A. Wedin. 2002. Mechanisms of plant species impacts on ecosystem nitrogen cycling. Ecology Letters 5:454–466.

Kunz, J. V., M. Rode, and R. Hensley. 2017. Water Resources Research. Journal of the American Water Resources Association 53:328–343.

Lorenzen, J., L. H. Larsen, T. Klær, and N. P. Revsbech. 1998. Biosensor determination of the microscale distribution of nitrate, nitrate assimilation, nitrification, and denitrification in a diatom- inhabited freshwater sediment. Applied and Environmental Microbiology 64:3264–3269.

Menzel, D. W., and R. F. Vaccaro. 1964. The measurement of dissolved organic and particulate carbon in seawater. Limnology and Oceanography 9:138–142.

Montana DEQ. 2018. Miller Creek Watershed Restoration Plan.

Moore, T. S., M. D. DeGrandpre, C. L. Sabine, R. C. Hamme, C. J. Zappa, W. R. McGillis, R. A. Feely, and W. M. Drennan. 2011. Sea surface pCO2 and O2 in the Southern Ocean during the austral fall, 2008. Journal of Geophysical Research: Oceans 116:1–12.

Mulholland, P. J., S. A. Thomas, H. M. Valett, J. Beaulieu, and J. R. Webster. 2006. Effects of light on NO3 uptake in small forested streams : diurnal and day-to-day variations. North American Benthological Society 25:583–595.

Murphy, T. P. 1980. Ammonia and Nitrate Uptake in the Lower Great Lakes. Canadian Journal of Fisheries and Aquatic Sciences 37:1365–1372.

Parker, S. R., S. R. Poulson, M. G. Smith, C. L. Weyer, and K. M. Bates. 2010. Temporal variability in the concentration and stable carbon isotope composition of dissolved inorganic and organic carbon in two montana, USA rivers. Aquatic Geochemistry 16:61–84.

Redfield, A. C. 1958. The biological control of chemical factors in the environment. American Scientist 46:230A, 205–221.

Roberts, B. J., and P. J. Mulholland. 2007. In-stream biotic control on nutrient biogeochemistry in a forested stream, West Fork of Walker Branch. Journal of Geophysical Research: Biogeosciences 112:1–11.

Roberts, B. J., P. J. Mulholland, and W. R. Hill. 2007. Multiple scales of temporal variability in ecosystem metabolism rates: Results from 2 years of continuous monitoring in a forested headwater stream. Ecosystems 10:588–606.

Simpson, G. L. 2017. Generalized additive models: An introduction with R. Second edition. CRC Press, Boca Raton, FL.

Simpson, G. L. 2018. Modelling palaeoecological time series using generalised additive models. Frontiers in Ecology and Evolution 6:1–21.

Smith, S. V, and J. T. Hollibaugh. 1993. Coastal metabolism and the oceanic organic carbon balance. Reviews of Geophysics 31:75–89.

Sokal, R. R., and F. J. Rohlf. 1994. Biometry: the principles and practices of statistics in biological research. Third edition. W. H. Freeman.

Steinman, A. D., G. A. Lamberti, and P. R. Leavitt. 2017. Biomass and Pigments of Benthic Algae. Pages 223–240 *in* F. R. Hauer and G. A. Lamberti, editors. Methods in Stream Ecology. London, United Kingdom.

Sullivan, A. B., J. I. Drever, and D. M. McKnight. 1998. Diel variation in element concentrations, Peru Creek, Summit County, Colorado. Journal of Geochemical Exploration 64:141–145.

U.S. EPA. 1993a. Method 353.1, Revision 2.0: Determination of nitrate-nitrite nitrogen by automated colorimetry. Cincinnati, Ohio.

U.S. EPA. 1993b. Method 365.1, Revision 2.0: Determination of phosphorus by semi-automated colorimetry. Cincinnati, Ohio.

U.S. EPA. 1993c. Method 350.1: Determination of ammonia nitrogen by semi-automated colorimetry. Cincinnati, Ohio.

Valett, H. M., S. A. Thomas, P. J. Mulholland, J. R. Webster, C. N. Dahm, C. S. Fellows, C. L. Crenshaw, and C. G. Peterson. 2008. Endogenous and Exogenous Control of Ecosystem Function: N Cycling in Headwater Streams. Ecology 89:3515–3527.

Webster, J. R., and J. L. Meyer. 1997. Organic Matter Budgets for Streams : A Synthesis. Journal of the North American Benthological Society 16:141–161.

Woelber, B., M. P. Maneta, J. Harper, K. G. Jencso, W. Payton Gardner, A. C. Wilcox, and I. López-Moreno. 2018. The influence of diurnal snowmelt and transpiration on hillslope throughflow and stream response. Hydrology and Earth System Sciences 22:4295–4310.

Wondzell, S. M., M. N. Gooseff, and B. L. McGlynn. 2007. Flow velocity and the hydrologic behavior of streams during baseflow. Geophysical Research Letters 34:1–5.

Yang, F., K. Ichii, M. A. White, H. Hashimoto, A. R. Michaelis, P. Votava, A. X. Zhu, A. Huete, S. W. Running, and R. R. Nemani. 2007. Developing a continental-scale measure of gross primary production by combining MODIS and AmeriFlux data through Support Vector Machine approach. Remote Sensing of Environment 110:109–122.

Supporting information

Nitrate uptake model

I derived the model for daily NO_3-N uptake areal flux (U_{ANO3}, mg N m^{-2} d^{-1}) from changes in NO_3-N concentration over time attributed to assimilatory autotrophic uptake ($\frac{\Delta N}{\Delta t}$, mg N m^{-3} d^{-1}). Deviation from ambient background NO_3-N concentration ($[N]_{dev}$, mg N m^{-3}) due to denitrification and upstream inputs was represented by a temporal NO_3-N rate, K (d^{-1}). Changes in stream flow were included by multiplying by stream depth, z (m):

$$U_{ANO3} = \left(\frac{\Delta N}{\Delta t} + K\,[N]_{dev}\right) z \quad (1)$$

Divide daily uptake areal flux by z to convert into a volumetric flux:

$$\frac{U_{ANO3}}{z} = \frac{\Delta N}{\Delta t} + K\,[N]_{dev} \quad (2)$$

Rearrange terms to solve for $\frac{\Delta N}{\Delta t}$:

$$\frac{\Delta N}{\Delta t} = \frac{U_{ANO3}}{z} - K\,[N]_{dev} \quad (3)$$

Take $\frac{\Delta N}{\Delta t}$ between each timestep i and the preceding timestep i-1:

$$\frac{([N]_i - [N]_{i-1})}{(\Delta t)} = \left(\frac{U_{ANO3}}{z_i} - K\,[N]_{dev}\right) \quad (4)$$

Rearrange the equation to solved for $[N]_{t_1}$:

$$[N]_i = [N]_{i-1} + \left(\frac{U_{ANO3}}{z_i} - K\,[N]_{dev}\right)(\Delta t) \quad (5)$$

I partitioned $\frac{U_{ANO3}}{z_i}$ with modeled light at each timestep ($PPFD_i$, µmol m^{-2} h^{-1}) from the beginning (u_0) and end (u_1) of each day (h), and integrated sunlight ($PPFD_u$, µmol m^{-2}) over continuous time u within each day (d):

$$[N]_i = [N]_{i-1} - \left(\frac{U_{ANO3}}{z_i}\right)\left(\frac{(u_1-u_0)\times PPFD_i}{\sum_{u=1}^{n} PPFD_u}\right) + K\,[N]_{dev}\,(\Delta t) \quad (8)$$

Deviation in concentration due to denitrification and upstream input, $[N]_{dev}$, was equal to the difference between background concentration, $[N]_b$ (mg N m^{-3}), and $[N]_{i-1}$:

$$[N]_i = [N]_{i-1} - \left(\frac{U_{ANO3}}{z_i}\right)\left(\frac{(u_1-u_0)\times PPFD_t}{\sum_{u=1}^{n} PPFD_u}\right) + K\,([N]_b - [N]_{i-1})\,(\Delta t) \quad (9)$$

Supporting figures

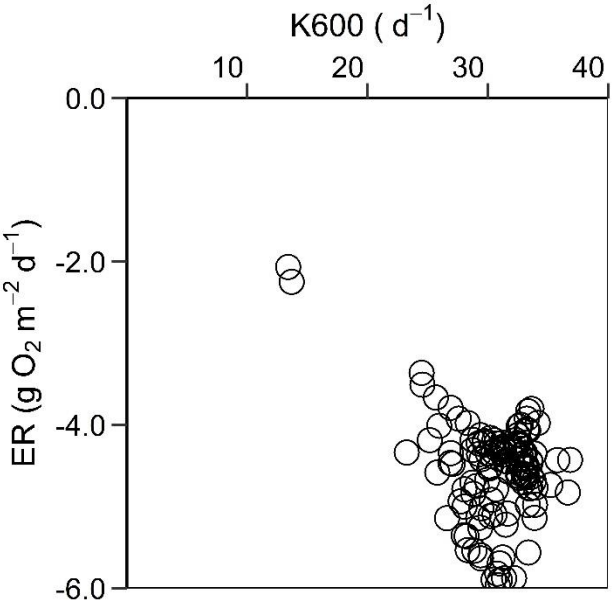

Fig. A.1. Median daily gas exchange rate (K600) and ER.

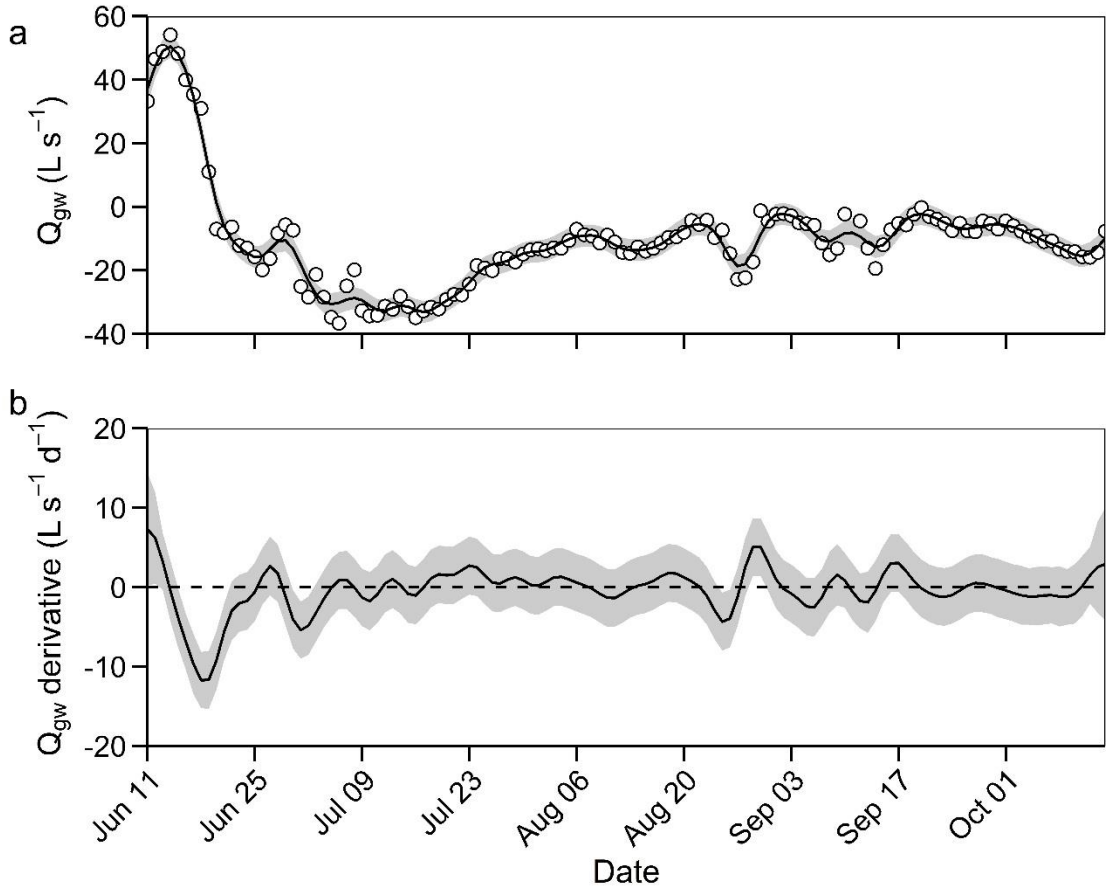

Fig.A.2. (a) Best-fit GAM (black line) of daily groundwater discharge (open circles) with 95% confidence intervals (gray bands) and **(b)** first derivative of the model (black line) with 95% simultaneous confidence intervals (gray bands) from June to October. Periods of change in Q_{gw} are indicated by derivative confidence intervals that do not include zero.

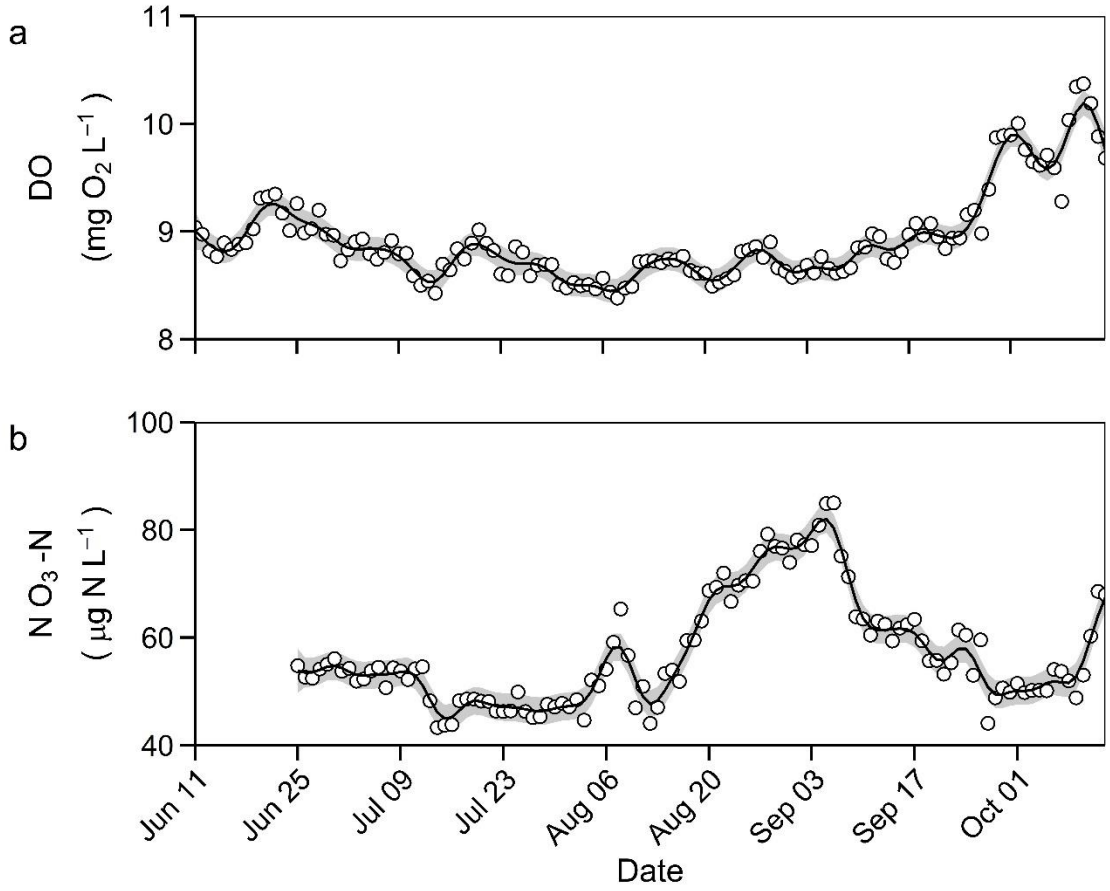

Fig.A.3. Comparison of modeled trends (black lines) in **(a)** observed (open circles) daily DO and **(b)** NO_3-N concentrations with 95% confidence intervals (gray bands).

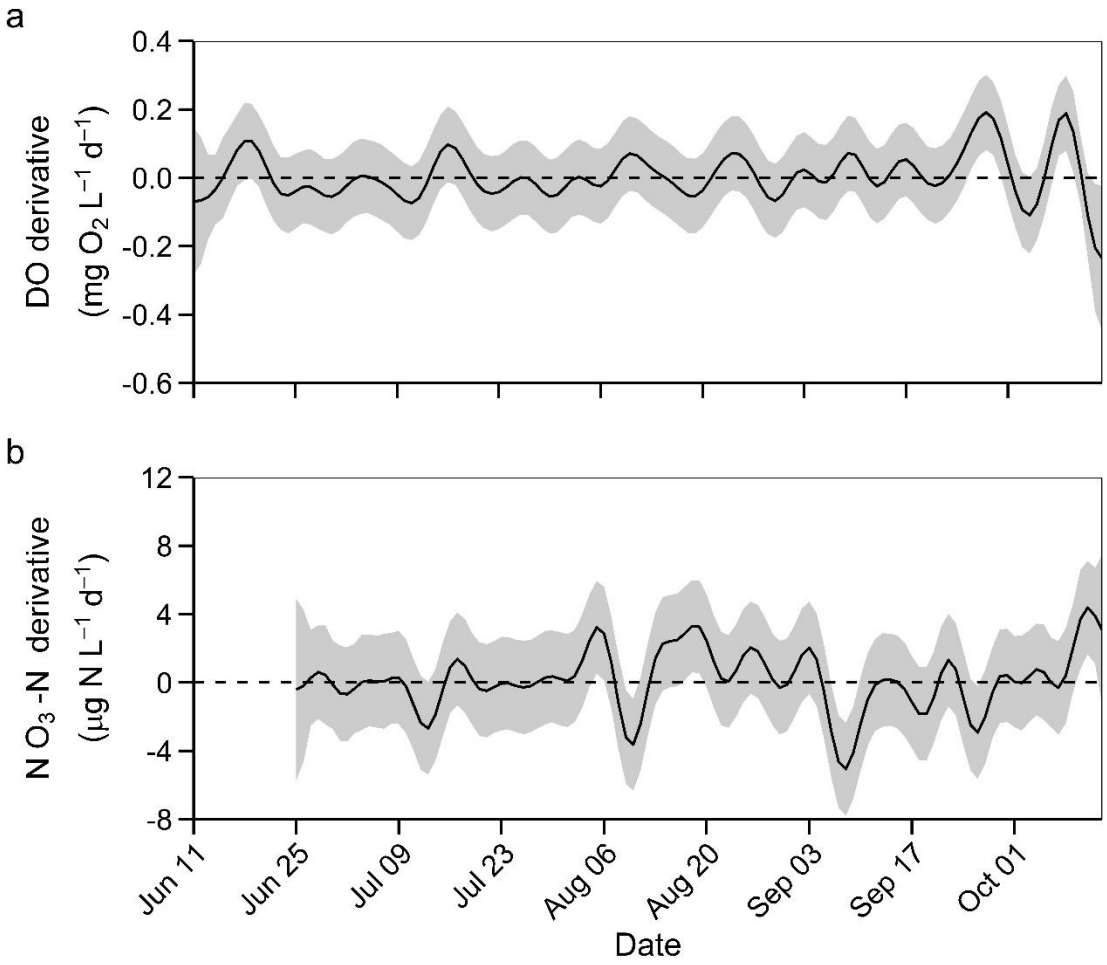

Fig.A.4. First derivatives (black lines) of **(a)** daily DO and **(b)** NO_3-N concentrations with 95% simultaneous confidence intervals (gray bands).

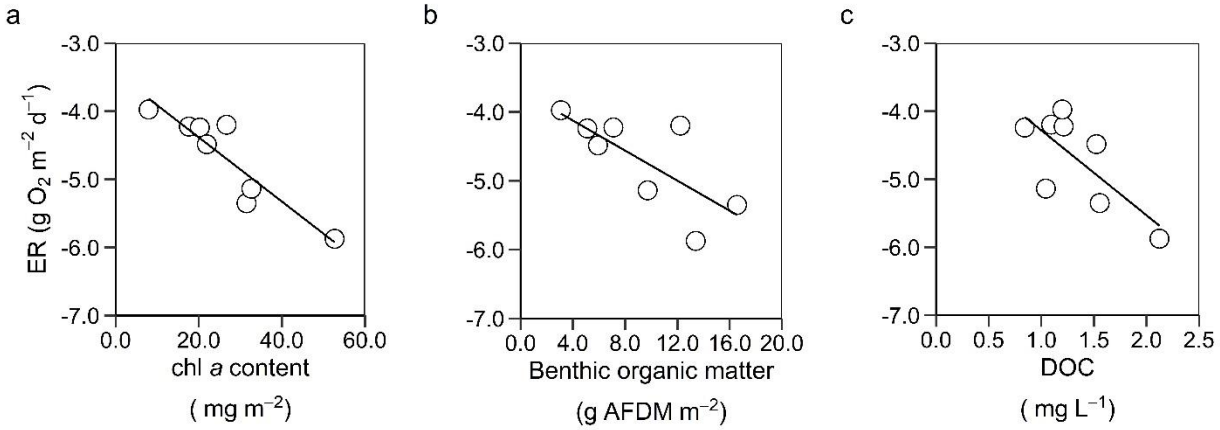

Fig. A.5. Relationships between ER and reach-average benthic standing stock metrics of **(a)** chlorophyll *a* content and **(b)** organic matter measured with AFDM, and **(c)** surface water DOC concentration. Lines denote best-fit linear regression.

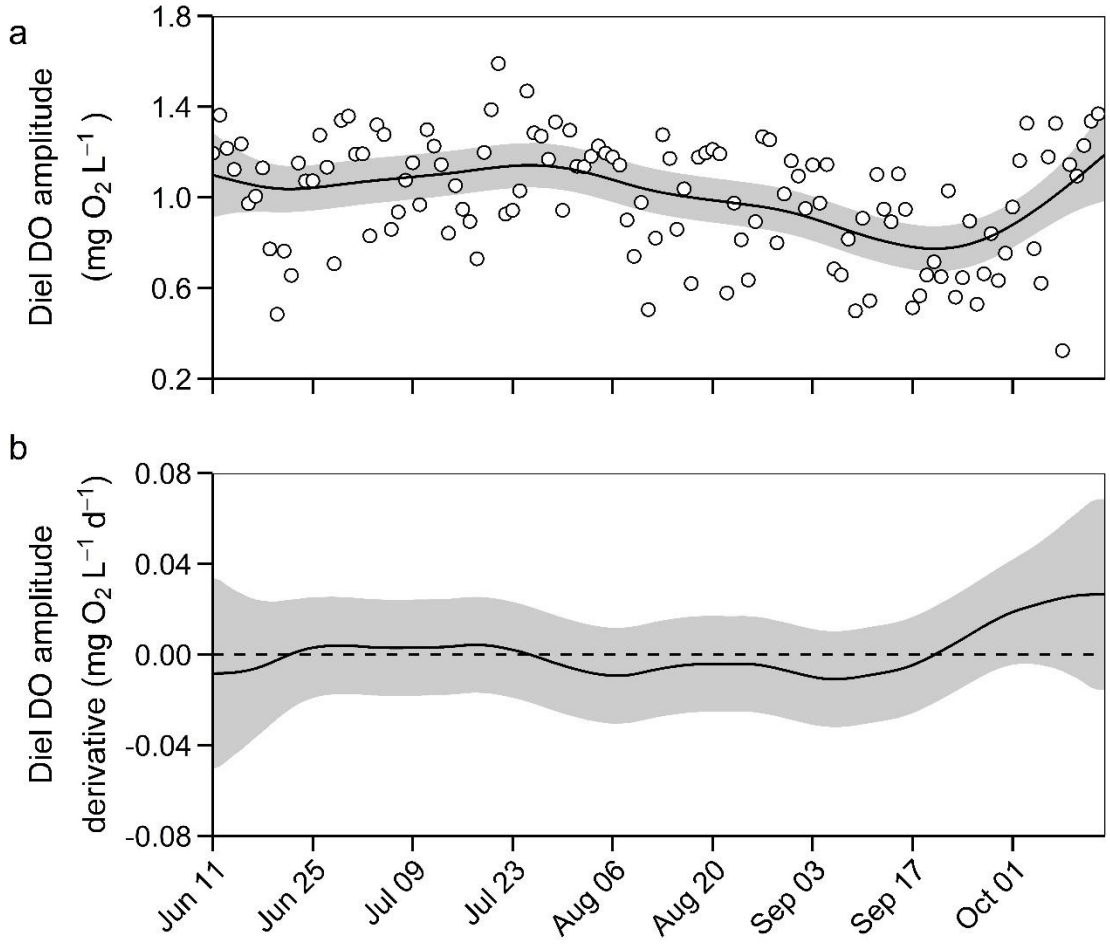

Fig. A.6. (a) Diel DO amplitude (open circles) and 95 % confidence intervals (gray bands) over the growing season. **(b)** Derivative (black line) with 95% simultaneous confidence intervals (gray bands) indicated that there were no points of change in DO amplitude.

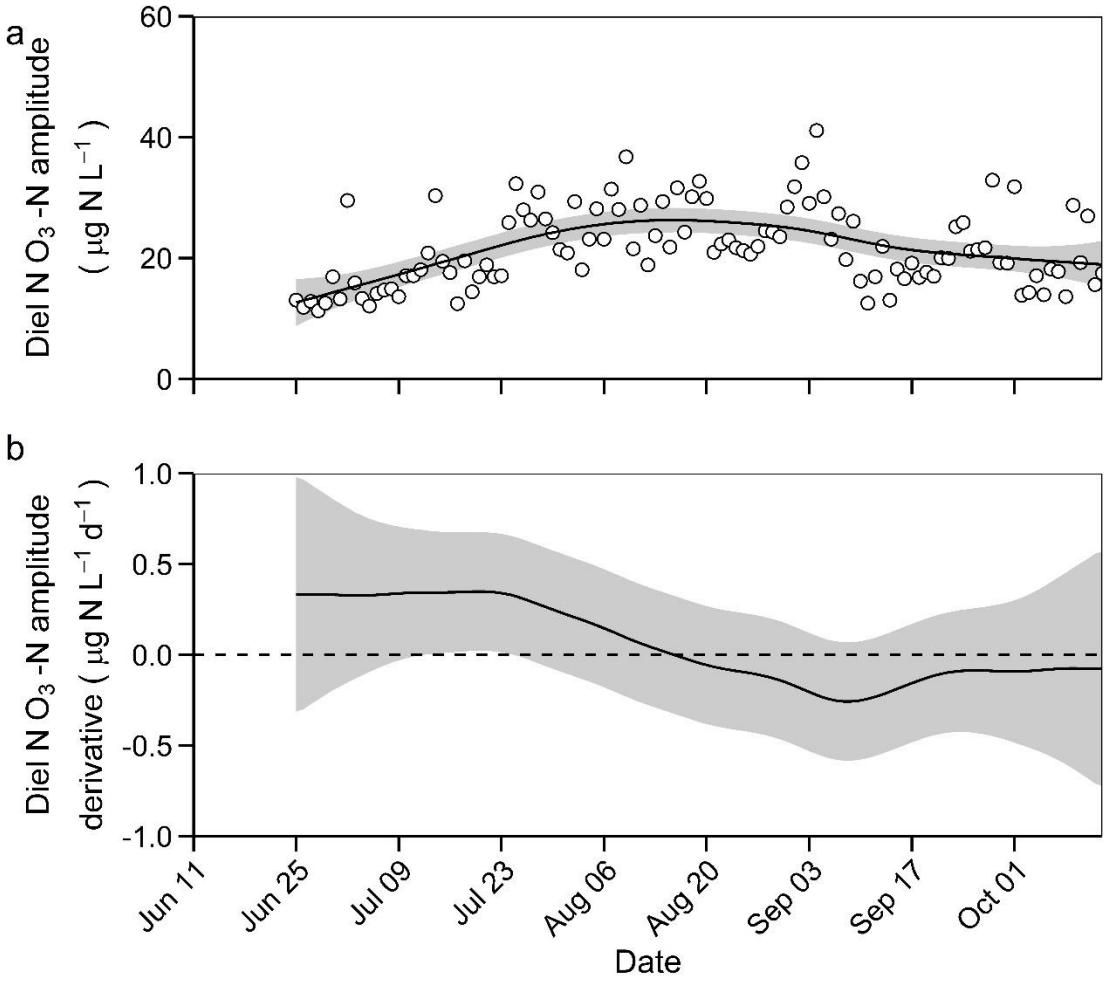

Fig. A.7. Growing season patterns in **(a)** diel NO_3-N amplitude (open circles) and 95 % confidence intervals (gray bands). **(b)** Derivative (black line) with 95% simultaneous confidence intervals (gray bands).

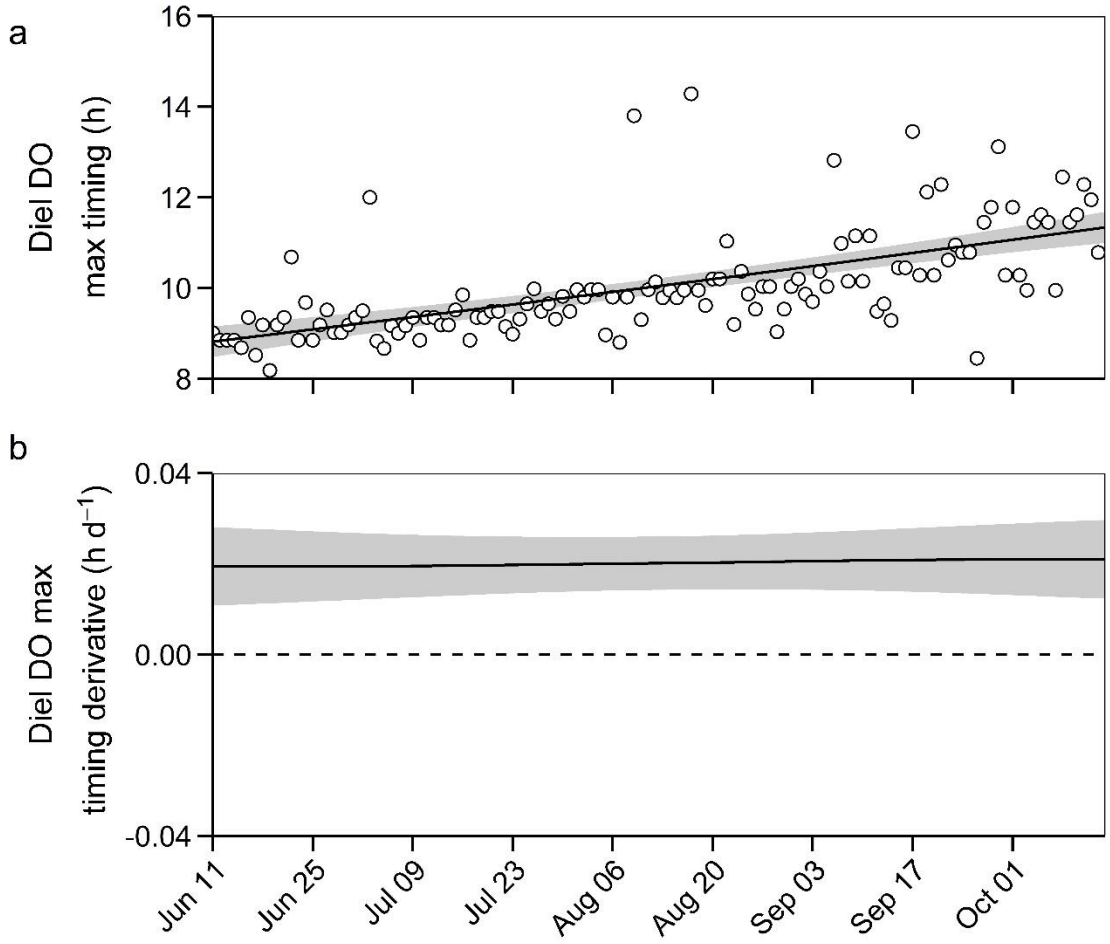

Fig. A.8. Diel timing of **(a)** DO maximum (open circles) with GAM (black line) and 95 % confidence intervals (gray bands) occurred later in the day as the study progressed, as indicated by positive **(b)** derivative with 95% simultaneous confidence intervals (gray bands).

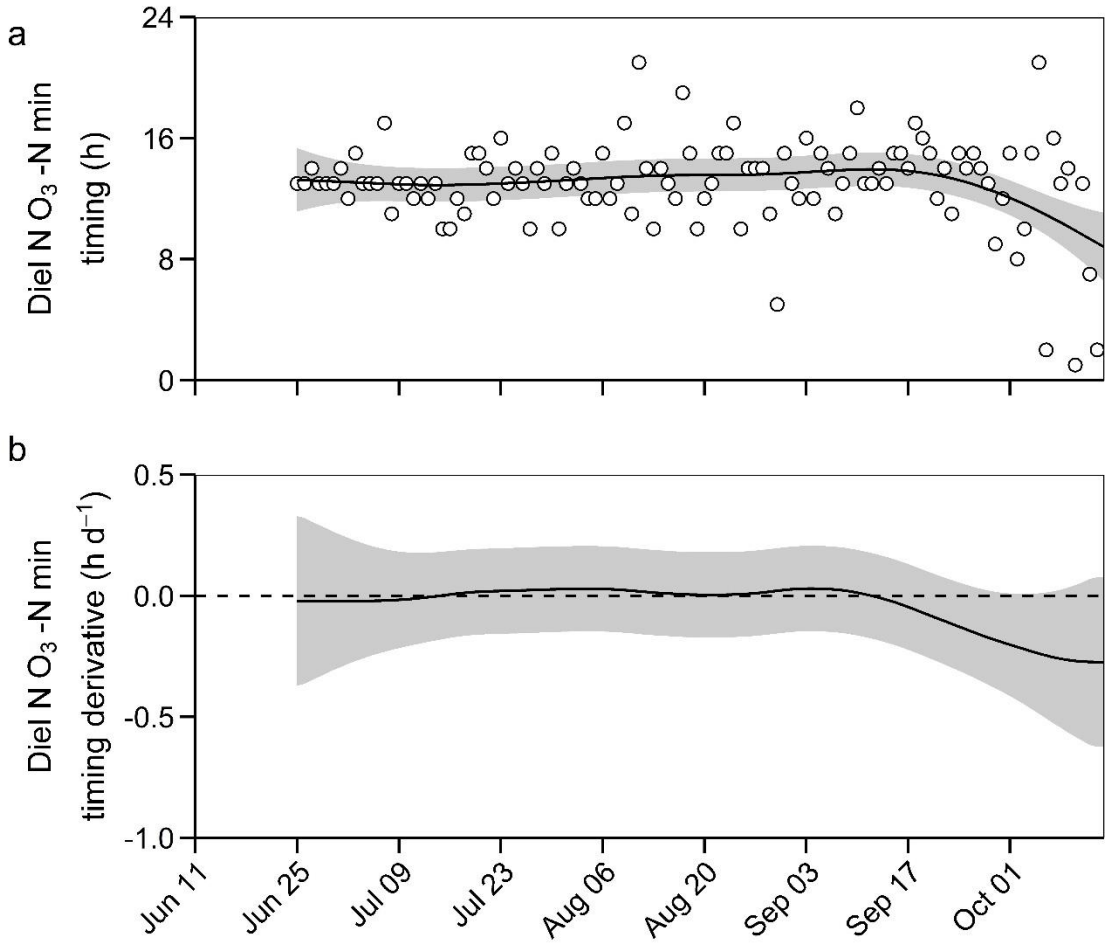

Fig. A.9. Diel timing of **(a)** NO_3-N minimum (open circles) with GAM (black line) and 95 % confidence intervals (gray bands) and **(b)** derivative with 95% simultaneous confidence intervals (gray bands) during the study.